Cytometry PART A
Journal of the International Society for Advancement of Cytometry

Polarized Light-Scattering Profile—Advanced Characterization of Nonspherical Particles with the Scanning Flow Cytometry

Dmitry I. Strokotov,[1,2] Alexander E. Moskalensky,[1,2] Vyacheslav M. Nekrasov,[1,2] Valeri P. Maltsev[1,2]*

[1]Institute of Chemical Kinetics and Combustion, Novosibirsk 630090, Russia

[2]Novosibirsk State University, Novosibirsk 630090, Russia

Received 6 December 2010; Revision Received 3 April 2011; Accepted 5 April 2011

Grant sponsor: Russian Ministry of Education and Science; Grant numbers: P422, P2497, P1039, 14.740.11.0729; Grant sponsor: Siberian Branch of the Russian Academy of Science; Grant numbers: 2009-37, 2009-7; Grant sponsor: Presidium of the Russian Academy of Science; Grant number: 2009-27-15; Grant sponsor: The President of the Russian Federation Programme for State Support of the Leading Scientific Schools; Grant number: NSh-65387.2010.4

*Correspondence to: Valeri Maltsev, Institute of Chemical Kinetics and Combustion, Institutskaya 3, Novosibirsk 630090, Russia

Email: maltsev@kinetics.nsc.ru

Published online in Wiley Online Library (wileyonlinelibrary.com)

DOI: 10.1002/cyto.a.21074

Abstract

We instrumentally, theoretically, and experimentally demonstrate a new approach for characterization of nonspherical individual particles from light scattering. Unlike the original optical scheme of the scanning flow cytometer that measures an angle-resolved scattering corresponding in general to S_{11} element of the light-scattering matrix, the modernized instrument allows us to measure the polarized light-scattering profile of individual particles simultaneously. Theoretically, the polarized profile is expressed by the combination of a few light-scattering matrix elements. This approach supports us with additional independent data to characterize a particle with a complex shape and an internal structure. Applicability of the new method was demonstrated from analysis of polymer bispheres. The bisphere characteristics, sizes, and refractive indices of the each sphere composing the bisphere were successfully retrieved from the solution of the inverse light-scattering problem. The solution provides determination of the Eulerian angles, which describe the orientation of the bispheres relatively to direction of the incident laser beam and detecting polarizer of the optical system. The both ordinary and polarized profiles show a perfect agreement with *T*-matrix simulation resulting to 50-nm precision for sizing of bispheres. © 2011 International Society for Advancement of Cytometry

Key terms

light scattering; inverse light-scattering problem; scanning flow cytometry; global optimization; T-matrix simulation; polarization; Eulerian angles; bisphere characterization

Polarization measurements have been widely used for analysis of particles (1–4). Usually, only the intensity of light scattered by a particle or an ensemble of particles is detected. An analysis of individual microscopic particles assumes a solution of identification and characterization problems. These problems can be solved from measurement of light-scattering intensity just for particles described by a simple optical model. To solve identification and especially characterization problems for particles described by a complex optical model, it is necessary to measure additional information. The polarizing measurement of scattering supports the solution with extra independent information required. In particular, polarization of scattered light is sensitive to deviations of a particle shape from spherical symmetry (5).

There are a large number of studies devoted to measurement of the polarization of light scattered by an ensemble of particles in suspension (6–12) and in aerosols (13–15). However, an analysis of data measured does not take into account the distribution functions over particle characteristics, because complexity of the analysis is incredibly increased. Also, there are few articles devoted to measuring the polarization of light scattered by single particles. The pioneering efforts of Phillips et al. (16) produced a measurement of light scattering by a single polystyrene sphere in the air

as a continuous function of scattering angle, and the incident radiation was linearly polarized. The authors also solved the problem of the characterization and obtained the size and the refractive index of polystyrene spheres. However, the measurement of one particle required a very long time (several hours). Using the same method, the polarization signal was measured from single airborne bacteria (17). The airborne bacterium was electrostatically trapped within the area of measurements. In this case, the intensity of scattered laser radiation was recorded by a movable detector in the range of scattering angles $\sim 7^{\circ}$–172°. The scattering function was measured for different polarizations of the incident radiation, as well as the signal of depolarization of single bacteria. In this article, the authors also attempted to solve the problem of characterization, but the measurement time for one bacterium was substantially large.

de Grooth et al. (18) suggested to measure the orthogonal depolarized light scattering as an additional parameter for flow cytometry. It was shown that the depolarization, caused by anisotropic cell structures and multiple scattering processes inside the cell, allows to distinguish between cell populations, in particular, to distinguish eosinophils from other granulocytes, and this effect was explained by numerical simulations (19). The author successfully solved the identification problem measuring scattering in the two solid angles, but a solution of the characterization problem requires much more scattering data to be discovered. Later Sloot et al. (20) demonstrated the possibility of measuring combinations of Mueller matrix elements on a flow cytometer measuring the polarization of the scattered radiation from the polystyrene microspheres. For this purpose, forward scattering, side scattering, and backward scattering channels were equipped by polarizers and depending on their position could detect different combinations of Mueller matrix elements. The polarization signal was measured only at fixed scattering angles.

There exist two levels of scientific description of particles in a disperse media: identification and characterization. Identification (also known as classification) means attributing the particles to one of several (usually predefined) classes from experimentally measured signals. Characterization means quantitative measurement of a particle by its morphological and functional characteristics, which can be retrieved from a solution of the inverse problem. Evidently, that characterization requires substantial scientific research to establish a mathematical relation between experimental signals and morphological characteristics of a particle. Most of the earlier mentioned articles relate to the solution of identification problem, and only four articles form the pool of papers where the characterization problem has been solved for blood cells using light scattering in flow cytometers (21–24). The main difficulty in solution of the inverse light-scattering (ILS) problem relates to development of an adequate optical model of a cell whose characteristics must be retrieved from the solution. The optical models developed in these studies were rather simple and could not properly describe a complexity of form and inner structure of cells. From the other hand, the flow cytometry supports a solution of the ILS problem only with forward and side scattering signals in ordinary configuration and angle-resolved dependence of S_{11} element for Mueller matrix with scanning flow cytometry (25). Developing more complex optical models and using them for solving of the ILS problem requires additional information on light scattering for cells. This activity is extremely important for hematology where a solution of the ILS problem could be used for more precise characterization of blood cells. The precise characterization of blood cells assumes measurements of not only concentrations that are inherent for modern hematological analyzers but also morphological characteristics such as volume, shape, density, and nucleus size.

In this article, we instrumentally, theoretically, and experimentally demonstrate a new approach for characterization of nonspherical individual particles from light scattering. We describe a new improved optical setup of the scanning flow cytometer (SFC) (26), which allows the measurement of the regular and polarized entire light-scattering profiles (LSPs) of individual particles. We also describe a data acquisition system for the SFC and data acquisition process that has been adapted for simultaneous measurement of the regular and polarized LSPs. The data acquisition system provides accurate measurement of these LSPs with a rate of 200 particles/s. Applicability of the new method for analysis of nonspherical particles was demonstrated from measurement of light scattering of polymer bispheres. The bisphere characteristics, sizes and refractive indices of the each sphere, were successfully retrieved from the solution of the ILS problem. The solution provides determination of the Eulerian angles, which describe the orientation of the bisphere relatively to direction of the incident laser beam and detecting polarizer of the optical system. The both ordinary and polarized LSPs show a perfect agreement with *T*-matrix simulation resulting to 50-nm precision for sizing of bispheres.

Materials and Methods

Sample Preparation

We used carboxylate-modified fluorescent microspheres (FluoSpheres® Fluorescent Microspheres, Cat. No. F-8827, actual size of 1.9 μm, Invitrogen Corp., Carlsbad, CA). The carboxylate-modified microsphere products are made by grafting polymers containing carboxylic acid groups to sulfate microspheres. The result is a microsphere with a highly charged, relatively hydrophilic and somewhat porous surface layer. The external layer produced by this modification process is only a few Ångstrom thick and therefore does not change the size of the seed particles. Carboxylate-modified microspheres are spontaneously aggregated forming bispheres (27) but much less strongly than the hydrophobic microspheres. The sample that contains monomers and dimers of spheres was measured with the modernized SFC.

Scanning Flow Cytometer: Optical Setup

The experimental work was performed with the instrumental platform of the universal analyzer for biology and medicine BioUniScan™ (CytoNova, Novosibirsk, Russian

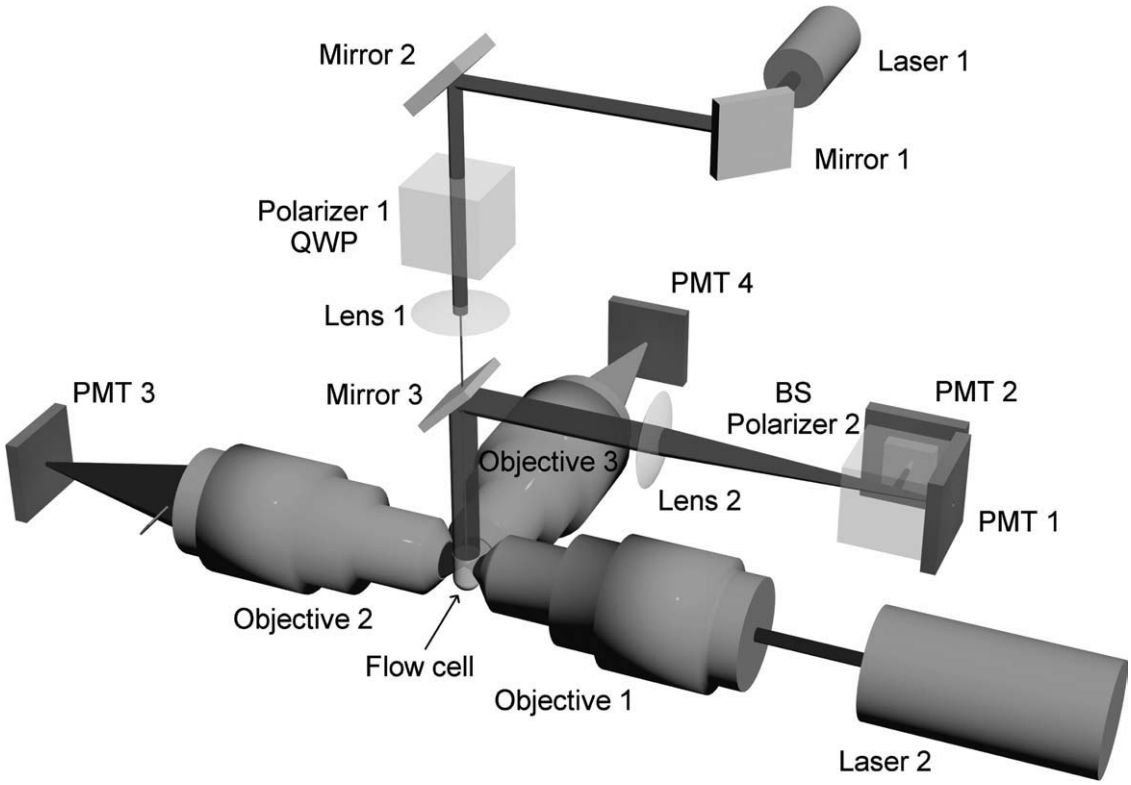

Figure 1. Schematic layout of the optical system of the modernized scanning flow cytometer.

Federation). The core of the BioUniScan is the SFC developed in Cytometry and Biokinetics Lab (Novosibirsk, Russian Federation) (25,26,28,29). The performance of the SFC in analysis of individual particles from light scattering was reviewed (30).

The schematic layout of the SFC optical system is presented in Figure 1. A diode laser (Laser 1, LM-660-20-S, 660 nm, 40 mW) was used for generation of the scattering pattern, and the orthogonal laser (Laser 2, Uniphase 2214-12SLAB, 488 nm, 25 mW) was used for excitation of fluorescence and for triggering the electronic unit. The beam of Laser 1 was directed coaxially with the stream by a lens (Lens 1, f =45 mm) through a hole in the mirror (Mirror 3). The Polarizer 1 and quart-wave plate (QWP) provide a circular polarization of the incident beam. The hydrofocusing head (not shown) produces two concentric fluid streams: a sheath stream without particles and a probe stream that carries the analyzed particles. Two syringes controlled by step motors form the sample flow. The fluidics system directs the streams into the capillary (diameter of 250 μm) of the flow cell (Fig. 1). Finally, analyzed particles are carried by the probe stream with a 12-μm diameter. Operational function of the optical scanning cuvette was previously described in detail (25,30). The light scattered by a single particle is reflected by Mirror 3 and directed by Lens 2 to the beam splitter (BS, nonpolarizing cube beamsplitter, Edmund Optics, PO: 001239). The BS splits beam with two parts, the first part is detected by photomultiplier tube (PMT) PMT 1 (Hammamatsu H9 305-04), and the second part passing through the Polarizer 2 is detected by PMT 2 (Hammamatsu H9 305-04). The beam of Laser 2 is focused by Objective 1 (NA = 0.2) into the capillary of the optical cell. The light scattered in the forward direction is collected by Objective 2 (NA = 0.2) and detected by PMT 3 (Hammamatsu H9 305-04). The beam stop prevents illumination of PMT 3 by the incoming laser beam. The fluorescence of dye molecules linked at a particle is collected by Objective 3 (NA = 0.4) and detected by PMT 4 (Hammamatsu H9 305-04). The band-pass optical filter provides measurement of the specific fluorescence with an appropriate signal-to-noise ratio. Actually, the PMT 4 schematically represents the fluorescence unit of the BioUniScan formed by dichroic mirrors and band-pass filters requested. The trigger signal that controls the SFC electronic unit can be generated from PMT 3 or from PMT 4.

The current optical setup of the SFC measures regular LSP and polarized LSP of individual particles. The angular resolution of the regular and polarized LSPs is better than 0.4°. Theoretical simulation of the LSPs will be introduced in the next section via Mueller matrix formalism.

Scanning Flow Cytometer: Mueller Matrix

In this section, the optical transfer function of the current measurement system i.e., lasers, polarizers, phase plate, particle, cuvette, and photo detectors, is described using the Mueller matrix formalism.

The complete information about the scattering from a particle can be presented in a form of a 4 × 4 Mueller matrix (light-scattering matrix) (31):

$$M = \begin{pmatrix} S_{11} & S_{12} & S_{13} & S_{14} \\ S_{21} & S_{22} & S_{23} & S_{24} \\ S_{31} & S_{32} & S_{33} & S_{34} \\ S_{41} & S_{42} & S_{43} & S_{44} \end{pmatrix} \quad (1)$$

where $S_{ij} = S_{ij}(\theta,\varphi)$ are the elements of Mueller matrix, and θ and φ are the polar and azimuthal angles of scattering, respectively. An electromagnetic field can be described via Stokes vector elements I, Q, U, and V (32):

$$\begin{pmatrix} I \\ Q \\ U \\ V \end{pmatrix} \quad (2)$$

The transformation of the Stokes vector of incident light by the polarizers and the phase plate, interaction with a particle within the optical system can be described by a corresponding Mueller matrix. The direction of the Polarizer 2 (Fig. 1) determines the basic coordinate system. The Mueller matrix of the Polarizer 2 that sets in 0°-orientation is as follows:

$$M_0 = \begin{pmatrix} 1 & 1 & 0 & 0 \\ 1 & 1 & 0 & 0 \\ 0 & 0 & 0 & 0 \\ 0 & 0 & 0 & 0 \end{pmatrix} \quad (3)$$

The Mueller matrix of the Polarizer 1 that sets in 90°-orientation is as follows:

$$M_{90} = \begin{pmatrix} 1 & -1 & 0 & 0 \\ -1 & 1 & 0 & 0 \\ 0 & 0 & 0 & 0 \\ 0 & 0 & 0 & 0 \end{pmatrix} \quad (4)$$

The Mueller matrix of the QWP is as follows:

$$M_{\mathrm{qwp}} = \begin{pmatrix} 1 & 0 & 0 & 0 \\ 0 & 1 & 0 & 0 \\ 0 & 0 & 0 & -1 \\ 0 & 0 & 1 & 0 \end{pmatrix} \quad (5)$$

The rotation of the basic coordinate system with angle φ is described by

$$M(\varphi) = \begin{pmatrix} 1 & 0 & 0 & 0 \\ 0 & \cos(2\varphi) & \sin(2\varphi) & 0 \\ 0 & -\sin(2\varphi) & \cos(2\varphi) & 0 \\ 0 & 0 & 0 & 1 \end{pmatrix}. \quad (6)$$

To evaluate the light scattering intensity on PMT 1, we have to multiply the matrices $M(-\varphi) \times M \times M(\varphi) \times M(-45) \times M_{\mathrm{qwp}} \times M(45) \times M_{90}$ with the vector $(1\ Q\ U\ V)^T$ (randomly polarized light) on the right side and with the vector (1 0 0 0) (photomultiplier) on the left side. Additionally, the result of multiplication must be integrated over azimuthal angle φ because of the spherical mirror of the optical scanning cuvette (25). The result of the multiplication and integration gives the regular LSP, and it is as follows:

$$I_{\mathrm{PMT1}}(\theta) = I_{\mathrm{r}}(\theta) = k \int_0^{2\pi} [S_{11}(\theta,\varphi) + S_{14}(\theta,\varphi)]d\varphi, \quad (7)$$

where k is the coefficient that depends on the SFC transfer function, the PMT 1 photon–electron conversion, and amplification of the SFC electronic circuit.

For the second channel of the SFC, the intensity measured by the PMT 2 is resulted from multiplication of the matrices $M_0 \times M(-\varphi) \times M \times M(\varphi) \times M(-45) \times M_{\mathrm{qwp}} \times M(45) \times M_{90}$ with the same vectors and is proportional to the following combination of the elements of the scattering matrix:

$$I_{\mathrm{PMT2}}(\theta) = k_1 \int_0^{2\pi} [S_{11}(\theta,\varphi) + S_{14}(\theta,\varphi) + (S_{21}(\theta,\varphi) + S_{24}(\theta,\varphi))\cos(2\varphi) - (S_{31}(\theta,\varphi) + S_{34}(\theta,\varphi))\sin(2\varphi)]d\varphi, \quad (8)$$

where k_1 is the coefficient that depends on the SFC transfer function, the PMT 2 photon–electron conversion, and amplification of the SFC electronic circuit. By means of the electronic circuit of the SFC, the coefficients k [Eq. (7)] and k_1 [Eq. (8)] were set equal k. The same electronic circuit subtracts $I_{\mathrm{PMT1}}(\theta)$ and $I_{\mathrm{PMT2}}(\theta)$ finalizing the SFC output: the regular LSP—$I_r(\theta)$ [Eq. (7)] and polarized LSP $I_p(\theta) = I_{\mathrm{PMT2}}(\theta) - I_{\mathrm{PMT1}}(\theta)$. Finally, the current SFC allows the measurement two independent combinations of Mueller matrix elements:

$$I_r(\theta) = \int_0^{2\pi} [S_{11}(\theta,\varphi) + S_{14}(\theta,\varphi)]d\varphi$$

$$I_p(\theta) = \int_0^{2\pi} [(S_{21}(\theta,\varphi) + S_{24}(\theta,\varphi))\cos(2\varphi) - (S_{31}(\theta,\varphi) + S_{34}(\theta,\varphi))\sin(2\varphi)]d\varphi. \quad (9)$$

We have to note that $\int_0^{2\pi} S_{14}(\theta,\varphi)d\varphi = 0$ for a particle with an axis of symmetry (33).

The important peculiarity of the SFC relates to measurement of light scattering of spherical particles. The elements of scattering matrix (1) do not depend on azimuthal angle φ and element $S_{14} \equiv 0$ for a spherical particle (31) that results to the following:

$$I_{\mathrm{r}}(\theta) = 2\pi S_{11}$$

$$I_{\mathrm{p}}(\theta) = 0. \quad (10)$$

The Eq. (10) demonstrates a new performance of the SFC, direct identification of nonspherical particles from light scattering. The signal I_p must exceed the noise level for a nonspherical particle. We tested this feature of the SFC experimentally with measurement of spheres and bispheres.

Additionally, we tested the performance of the SFC in measurement of the polarized LSP from analysis of spheres removing the QWP from the optical setup. Instead of subtrac-

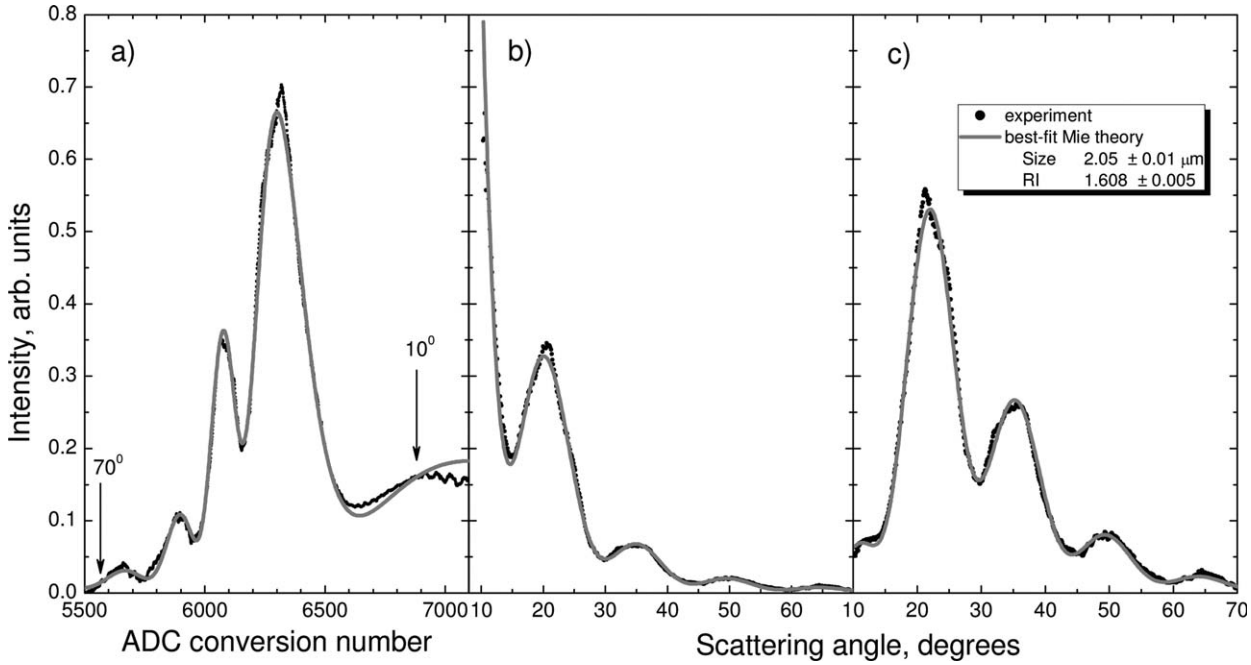

Figure 2. The light-scattering trace (**a**), the light-scattering profile (**b**), and the weighted light-scattering profile (**c**) of an individual sphere. The points and lines relate to experimental data and to best-fit simulation from Mie theory, respectively. The arrows in (a) approximately indicate ADC conversion numbers for scattering angles of 10° and 70°. The best-fit profile corresponds to the sphere with parameters shown in the box.

tion of signals from PMT 1 and PMT 2 described earlier, we divided the PMT 2 signal by PMT 1. In this arrangement, the polarized LSP becomes the following combination of the matrix elements (a spherical particle):

$$I_p(\theta) \propto 1 - \frac{S_{33}}{S_{11}} \qquad (11)$$

Scanning Flow Cytometer: Data Acquisition System

The optical system of the SFC assumes measurement of four signals: trigger and fluorescence pulses (PMT 3 and PMT 4 in Fig. 1, respectively) as well as regular and polarized light-scattering traces (PMT 1 and PMT 2 in Fig. 1, respectively). Four Hamamatsu Photo Sensor modules H9305-04 were used for measurement of these signals. The module includes an amplifier and third-order low-pass filter with upper frequency limit on 4 MHz. The signals are further amplified and additionally filtered by second-order low-pass filter with similar frequency. All signals from PMTs are digitized by individual 14-bit analog–digital convertor (ADC) AD9240AS (Analog Devices). The data collection is started by the software, and it is running continuously with a 6.25-MHz sampling frequency synchronized for all ADCs. When a particle crosses the orthogonal beam zone, the trigger signal increases until it exceeds the threshold value that initialize the data transfer from ADCs to PC.

Measurement and control software is made using the National Instruments' LabView 8.2 graphical programming environment. LabView 8.2 runs currently on an IBM-PC compatible computer under the Windows XP SP2 operating system.

At the first stage, we acquire the regular light-scattering trace (LST) from PMT 1 (Fig. 1), where light-scattering intensity is shown as a function of ADC conversions (Fig. 2a). Then, the LST is transformed into the LSP by a multiplication with the normalizing coefficient of the SFC and a conversion of the ADC conversion numbers to scattering angles (Fig. 2b) (30). Actually, the ADC conversion numbers could be easily transformed into the measurement time by multiplication with the ADC conversion time of 0.16 μs. Finally, the LSP is modified by multiplication with a weighting function resulting to the

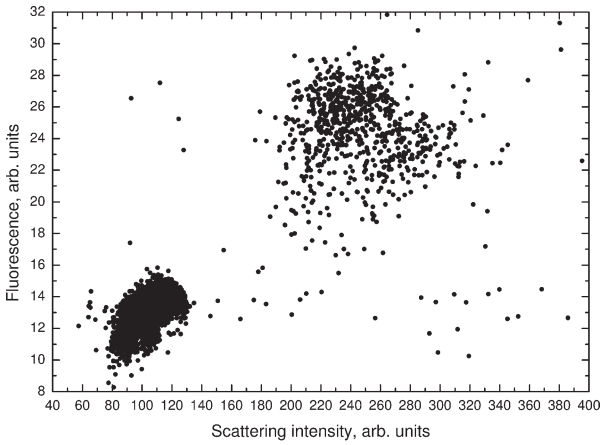

Figure 3. The fluorescence⊗scattering map of the sample that contains individual spheres and bispheres.

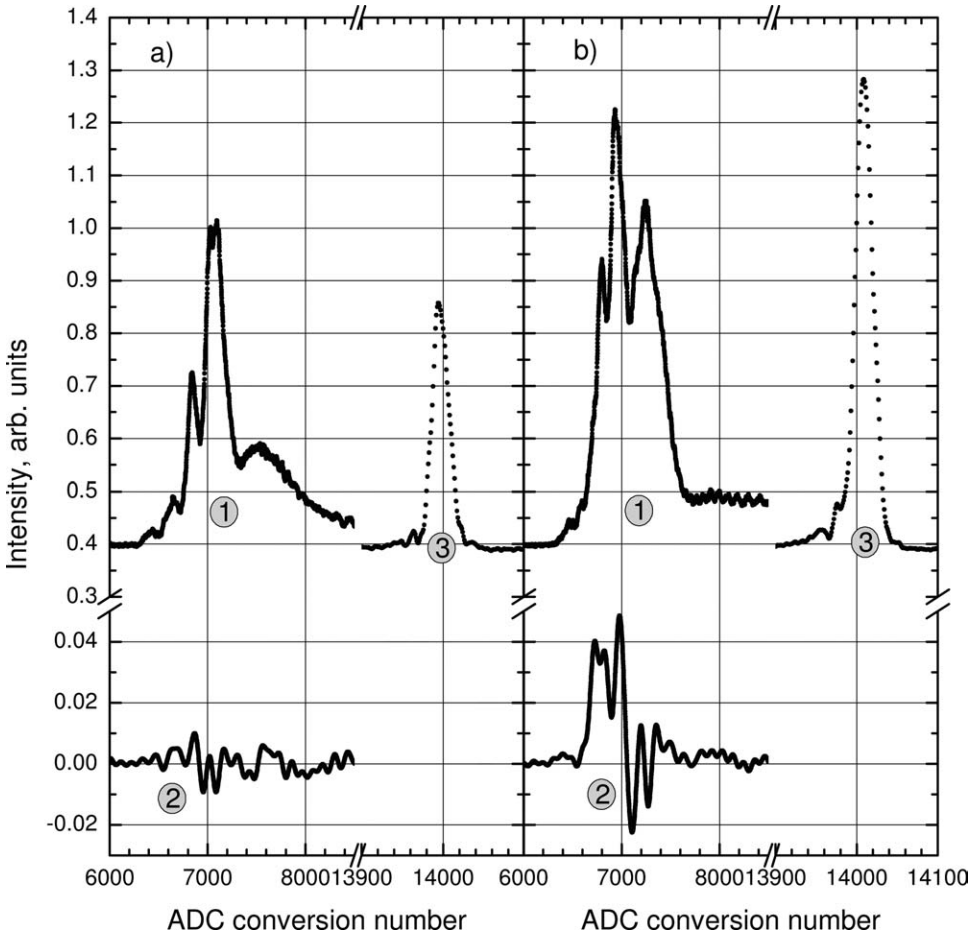

Figure 4. Light scattering and fluorescence signals from a sphere (**a**) and from a bisphere (**b**) measured with the scanning flow cytometer. Numbers relate to the following: 1: regular light-scattering trace; 2: polarized light-scattering trace; and 3: fluorescence pulse.

weighted LSP (wLSP) shown in Figure 2c. The weighting function is as follows:

$$w(\theta) = \frac{1^\circ}{\theta}\exp\left(-2\ln^2(\theta/54^\circ)\right) \qquad (12)$$

which is an approximate description of the normalizing coefficient of the SFC transfer function (30) by a log-normal function. The wLSP is similar to the LST with an inversion of abscissa axis (compare Figs. 2a and 2c). Actually, the weighting function provides a correct signal-to-noise ratio over region measured to fit an experimental data by theoretical simulations. These transformations were applied to the both regular and polarized LSTs.

Results

Verification of the SFC Alignment: Circular Polarization

To study the performance of the SFC in measurement of polarized properties of scattering from individual particles, we performed the verification of the SFC optical system alignment. First of all, we compare the S_{11} element of the matrix with the regular wLSP of the SFC. The result of the comparison is shown in Figure 2c. We found a perfect agreement between experimental measurement and theoretical simulation for a sphere within angular region ranging from 10° to 70°. The best-fit wLSP was evaluated by means of global optimization with DiRect algorithm (34) that allowed us to determine errors of characteristic estimates (24). We would like to emphasize the error in sizing of the sphere. The precision of 10 nm in sizing of the individual sphere is an extremely high value for optical methods.

According to statement (10), we performed a fine alignment of the laser beam and particle trajectory measuring LSTs of spheres. The measured sample contains individual spheres and bispheres (dimers). To classify monomers and dimers, we formed the fluorescence⊗scattering map, where fluorescence relates to an integral of the fluorescence pulse, and scattering relates to an integral of the regular LST. This map is presented in Figure 3. Dimers demonstrate doubled fluorescence and 2.5× scattering relatively to individual spheres. An accuracy of the SFC alignment was controlled by the polarized LST of spheres. The typical light-scattering data measured from a sphere is shown in Figure 4a. There are shown the regular LST-1, the polarized LST-2, and fluorescence pulse-3. Indeed the signal of polarized LST from a sphere is oscillated near

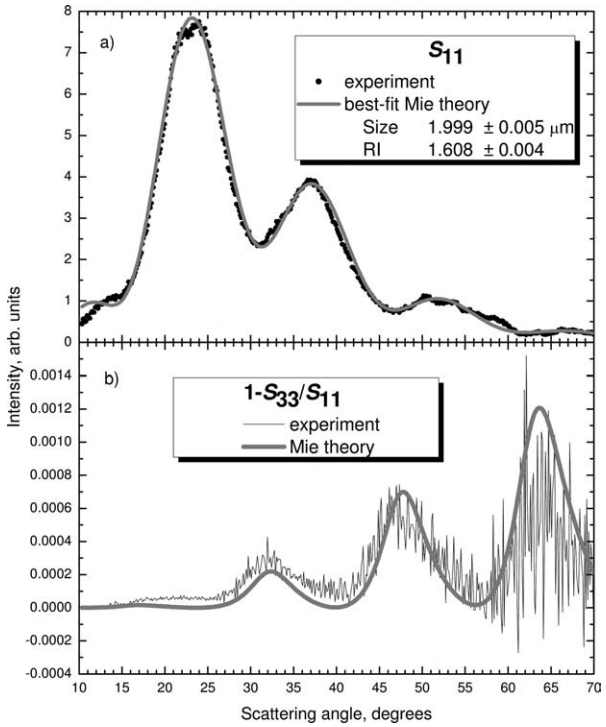

Figure 5. The regular weighted light-scattering profile of an individual sphere (**a**) and weighted light-scattering profile that corresponds to 1-S_{11}/S_{33} combination of the scattering matrix elements of the same sphere (**b**).

zero that corresponds to $I_p(\theta)$ from Eq. (10). This fact is an indicator of a correct alignment of the optical and hydrodynamic systems of the SFC.

The typical signal of a sphere dimer is presented in Figure 4b. There are also shown: the regular LST-1, the polarized LST-2, and fluorescence pulse-3. The polarized LST of the dimers substantially exceeded zero, and structure of the regular LST of the dimers was more complex than the regular LST of individual spheres.

Verification of the SFC Alignment: Linear Polarization

The polarized channel of the SFC gives us an additional test of agreement between experiment and Mie theory. We measured the same spheres without QWP in optical system of the SFC. The regular wLSP of a sphere is shown in Figure 5a. We have applied the DiRect algorithm to retrieve characteristics of the sphere from light scattering, and results are shown in the box of Figure 5a. Again our method results to 5-nm precision in a sphere sizing. The polarized wLSP that corresponds to Eq. (11) in this experiment is shown in Figure 5b. The measured polarized wLSP was simulated from Mie theory for the sphere with the characteristics determined from the regular wLSP. The result of the simulation is shown as a thick grey line in Figure 5b. There is a good agreement between experimental and theoretical data.

Analysis of Bispheres

We demonstrated the performance of the modified SFC to measure a polarized LSP of individual particles in the previous sections. In current section, we are using this advantage of the SFC in an analysis of nonspherical particles, e.g., bispheres. An analysis of a particle from light scattering assumes a solution of the ILS problem, i.e., determination of particle characteristics from light-scattering data. At present, solutions of the ILS problem are available for a sphere (25,35–37), an oblate spheroid in fixed orientation (23), and a coated sphere (24). In general, an accuracy of solutions of the ILS problem depends on amounts of input independent data and characteristics of a particle. The regular LSP can be successfully used in the solution of the ILS problem if an amount of particle characteristics is increased from two to four. If amount of particle characteristics exceeds four, the accuracy of the solution of the ILS problem drops dramatically down. More independent light-scattering data will be useful to solve the ILS problem for a particle with six characteristics like a bisphere. The solution of the ILS problem for a bisphere has to allow determination of the following characteristics: radii and refractive indices of two spheres composing dimer and two Eulerian angles. The Eulerian angles describe the orientation of a particle relatively to direction of the incident laser beam and default polarization of optical system. We solved the ILS problem for a bisphere using the global optimization with DiRect algorithm, where the *T*-matrix method (38) was applied to simulate light scattering from a bisphere.

We characterize a bisphere from the size parameters $x_{1,2} = \frac{\pi d_{1,2}}{\lambda} n_0$, where $d_{1,2}$ is the sizes of the spheres composing the dimer, λ is the wavelength of the incident laser beam, n_0 is the refractive index of surrounding medium, and the relative refractive indices $m_{1,2} = \frac{n_{1,2}}{n_0}$, where $n_{1,2}$ is the refractive indices of the spheres composing the dimer. The Eulerian angles are as follows: angle β is the angle between a direction of the dimer symmetry axis and direction of laser beam propagation (z-axis), and angle α is the angle between the projection of the dimer symmetry axis at x,y-plane and x-axis that coincides direction of detecting polarizer of the SFC optical system (Polarizer 2 in Fig. 1). We applied the DiRect algorithm varying the dimer characteristics in the following ranges: size parameter and relative refractive index of spheres composing dimer from 12 to 14 and from 1.12 to 1.24, respectively; angles α and β from 0° to 180° and from 0° to 90°, respectively. To use simultaneously the independent information contained in regular and polarized wLSP, the solving algorithm was realized in three stages. At the first stage, the DiRect algorithm was applied to the regular wLSP varying $x_{1,2}$, $m_{1,2}$, and angle β because the regular wLSP does not depend on the angle α. The four characteristics of the bisphere and angle β were retrieved from the first stage of the solution of the ILS problem. Then, we applied the DiRect algorithm to polarized wLSP varying the Eulerian angles and fixing the characteristics of the bisphere retrieved from the first stage. The second stage gave us angles α and β corrected. Additionally, we evaluated the mean standard error (MSE) for the experimental regular wLSP and best-fit *T*-matrix regular wLSP and the MSE for the experimental polarized wLSP and best-fit *T*-matrix polarized wLSP. The experimental points of the polarized wLSP were multiplied by a coefficient to equalize the MSEs calculated

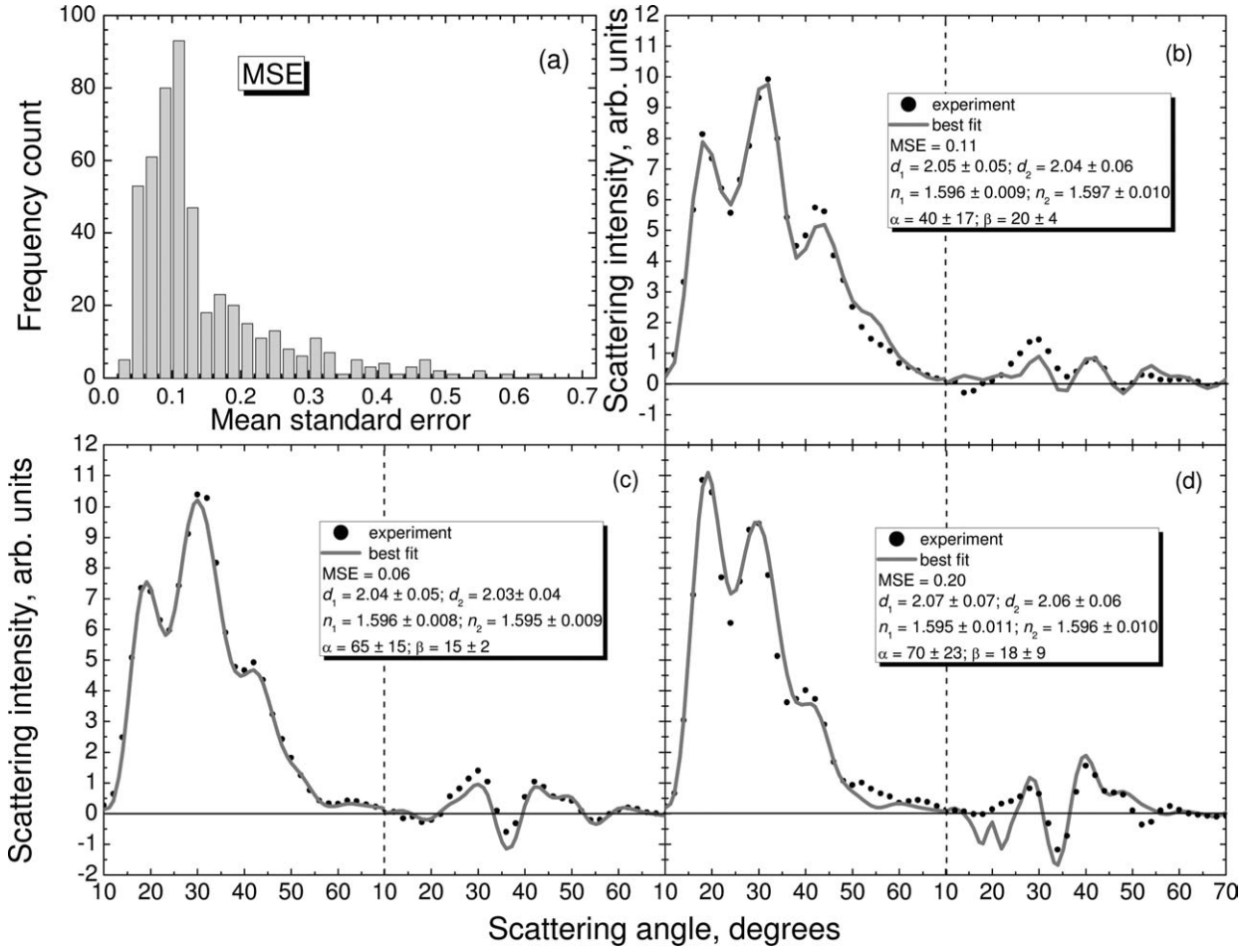

Figure 6. The mean standard error distribution of processing of the regular and polarized wLSPs of dimers with global optimization (**a**). The results of global optimization applied to merged regular and polarized wLSPs of bispheres (**b**), (**c**), and (**d**).

before. At the third stage of the solution, the regular and magnified polarized wLSPs were together merged, and the DiRect algorithm was applied for joint wLSP varying all six characteristics. Finally, the solution of the ILS problem for a single bisphere allows us to find the best-fit *T*-matrix wLSP to determine the four characteristics of the bisphere and the Eulerian angles. We analyzed 500 bispheres, and distribution of the MSE for the sample was formed (Fig. 6a). The results of the solution of the ILS problem for the three bispheres with the different MSEs are shown in Figures 6b–6d. There are the best-fit T-matrix wLSPs with the MSE, the characteristics of the bispheres, and the Eulerian angles for the each sphere in figures. The errors of determination of the bisphere characteristics and the Eulerian angles are also presented. The introduced global optimization with the DiRect algorithm takes ~60 min to process an individual bisphere using PC (LabView 8.2, 2.6 GHz processor).

Discussion

The results introduced in previous sections show a perfect agreement between experimental regular LSPs measured with SFC and LSP calculated from the Mie theory that results to sizing of individual spheres with a precision of few nanometers. An additional light-scattering channel of the SFC allowed us to measure the polarized LSPs of individual spheres. The main problem in measurement of polarized LSP is a rather weak signal. Fortunately, we reached 1% noise-to-signal ratio for the polarized signal relatively to regular ones, and polarized LSPs demonstrated a good agreement with the Mie theory in two series of experiments. First, a polarized LSP gives a nice tool for the proper alignment of the optical system of the SFC becoming zero for spherical particles. Second, the orthogonal arrangement of polarizers results to a really weak light-scattering signal, but we successfully measured the LSP that corresponded to the unique combination of the Mueller matrix elements.

Our preliminary simulations had shown that effects of depolarization caused by reflection by the capillary, the spherical mirror, and the 45°-mirror with a hole do not exceed 1% of the amplitude of the regular LSP. The additional distortion of the polarized LSP is resulted from a deviation of a particle trajectory from the capillary axis. Summarizing the polarized signal of spherical particles approximately two times exceeds statistical noise (see Fig. 4a). Nevertheless, we successfully

Table 1. Characteristics of the sample with monomer and dimer spheres retrieved from regular and polarized LSPs by means of solution of the ILS problem

CHARACTERISTICS	MONOMER SPHERES	DIMER SPHERES
Mean size (μm)	2.049 ± 0.001	2.050 ± 0.002
Standard deviation (μm)	0.043	0.066
Mean refractive index	1.5975 ± 0.0004	1.5975 ± 0.0005
Standard deviation	0.014	0.016
Mean Eulerian angle α (degrees)	–	93 ± 2
Standard deviation (degrees)	–	51
Mean Eulerian angle β (degrees)	–	18.4 ± 0.4
Standard deviation (degrees)	–	9

aligned the optical system of the SFC and measured the polarized LSP from bispheres. Moreover, this additional light-scattering data, i.e., polarized LSP, allowed us to solve the ILS problem for a bisphere resulting to detailed characterization of the sample (Table 1). The mean size of the dimer spheres was calculated from averaging of sizes of spheres composing the dimer in a sample. There are mean values ($\pm$ error of mean) and theirs standard deviations for a size, a refractive index, and Eulerian angles. The statistical results introduced in Table 1 demonstrate a perfect agreement between characteristics of the spheres retrieved from the two different solutions of the ILS problem. We are emphasizing the fact that the solutions are based on two different methods solving the direct light-scattering problem—Mie theory and *T*-matrix method. The monomer spheres were sized with a mean error of 13 nm over 1,000 spheres in the sample (standard deviation of 6 nm), whereas the dimer spheres were sized with a mean error of 49 nm (standard deviation of 11 nm). The similar ratio between the mean errors of determination of refractive indices: 0.006 (standard deviation of 0.002) and 0.013 (standard deviation of 0.005) for monomer and dimer spheres, respectively. The expected broadening of size distribution for dimer spheres comparing with monomer spheres is caused by difference in the errors of size estimates. There are also expected results with measured distribution of the Eulerian angles: the orientation of bisphere with angle α is equiprobable over the varying range of the angle, whereas the orientation of bispheres with angle β is rather narrow, and mean angle β lies close to 15°. The orientation at angle of 15° corresponds to a rotation of nonspherical particles in Poiseuille flow (25) within a flow channel of the SFC.

We performed an extremely important work for our team. The polarized LSP opens a way in searching of solutions of the ILS problem for cells with complex shapes and inner structures. We are able to model a cell with a body that can be mathematically described by means of six or even more parameters including orientation of the body. First of all, this approach looks very potential to characterize mature red blood cells (RBCs) from light scattering. A solution of the ILS problem for RBCs has to determine three RBC characteristics and two Eulerian angles that have nice perspectives with measurement of the polarized LSP. Implementation of this approach into a hematological analyzer allows an exclusion of RBC spherizing procedure that gives a substantial systematical error in RBC characterization (39). The polarized LSP will be very useful in analysis of homogeneity of nucleus of mononuclear cells to clarify the reason of heterogeneity of lymphocyte populations of humans (24). An analysis of dimer of blood platelets from light scattering could not be realized without measurement of the polarized LSP and even more combinations of Mueller matrix elements must be measured to reach a success in this study. The similar efforts must be applied in quantitative measurement of neutrophil granularity that plays an important role in detection of pathologies (40). This work gave a super-stimulus for our current research to be successful in earlier mentioned studies.

Acknowledgments

The author (VPM) thanks Prof. Erkki Soini (http://www.arcdia.com/arcdia-group/arctic-diagnostics/board) for the fruitful joint work with him in Finland 15 years ago when the first idea of polarized scanning flow cytometry was enthusiastically discussed.

Literature Cited

1. Lee J, Koh J, Collins RW. Multichannel Mueller matrix ellipsometer for real-time spectroscopy of anisotropic surfaces and films. Opt Lett 2000;25:1573–1575.
2. Sankaran V, Everett MJ, Maitland DJ, Walsh JT. Comparison of polarized light propagation in biological tissue and phantoms. Opt Lett 1999;24:1044–1046.
3. Nordin GP, Meier JT, Deguzman PC, Jones MW. Micropolarizer array for infrared imaging polarimetry. J Opt Soc Am A 1999;16:1168–1174.
4. Chou PC, Fini JM, Haus HA. Real-time principle state characterization for use in PMD compensators. IEEE Photon Technol Lett 2001;13:568–570.
5. Mishchenko MI, Travis LD. Polarization and depolarization of light. In: Moreno F, González F, editors. Lecture Notes in Physics. Lectures. 1998. LNP 534. Berlin: Springer-Verlag; 2000. p 159–175.
6. Bickel WS, Davidson JF, Huffman DR, Kilkson R. Application of polarization effects in light scattering: A new biophysical tool. Proc Natl Acad Sci U S A 1976;73:486–490.
7. Bickel WS, Stafford ME. Polarized light scattering from biological systems: A technique for cell differentiation. J Biol Phys 1981;9:53–66.
8. Bronk BV, Van De Merwe WP, Stanley M. In vivo measure of average bacterial cell size from a polarized light scattering function. Cytometry 1992;13:155–162.
9. Bronk BV, Druger SD, Czege J, Van De Merwe WP. Measuring diameters of rod-shaped bacteria in vivo with polarized light scattering. Biophys J 1995;69:1170–1177.
10. Van De Merwe WP, Li Z, Bronk BV, Czege J. Polarized light scattering for rapid observation of bacterial size changes. Biophys J 1997;73:500–506.
11. Van De Merwe WP, Czégé J, Milham ME, Bronk BV. Rapid optically based measurements of diameter and length for spherical or rod-shaped bacteria in vivo. Appl Opt 2004;43:5295–5302.
12. Ding H, Lu JQ, Brock RS, McConnell TJ, Ojeda JF, Jacobs KM, Hu XH. Angle-resolved Mueller matrix study of light scattering by B-cells at three wavelengths of 442, 633 and 850 nm. J Biomed Opt 2007;12:034032.
13. Hovenier JW, De Hann JF. Polarized light in planetary atmospheres for perpendicular directions. Astron Astrophys 1985;146:185–191.
14. Mukai S, Sano I, Takashima T. Investigation of atmospheric aerosols based on polarization measurements and scattering simulations. Opt Rev 1996;3:487–491.
15. Menghua Wang. Aerosol polarization effects on atmospheric correction and aerosol retrievals in ocean color remote sensing. Appl Opt 2006;45:8951–8963.

16. Phillips DT, Wyatt PJ, Berkman RM. Measurement of the Lorenz-Mie scattering of a single particle: Polystyrene latex. J Colloid Interface Sci 1970;34:159–162.
17. Wyatt PJ, Phillips DT. Structure of single bacteria from light scattering. J Theor Biol 1972;37:493–501.
18. de Grooth BG, Terstappen LWMM, Pupples GJ, Greve J. Light-scattering polarization measurements as a new parameter in flow cytometry. Cytometry 1987;8:539–544.
19. Yurkin MA, Semyanov KA, Maltsev VP, Hoekstra AG. Discrimination of granulocyte subtypes from light scattering: Theoretical analysis using a granulated sphere model. Opt Express 2007;15:16561–16580.
20. Sloot PMA, Hoekstra AG, Van Der Liet H, Figdor CG. Scattering matrix elements of biological particles measured in a flow through system: theory and practice. Appl Opt 1989;28:1752–1762.
21. Tycko DH, Metz MH, Epstein EA, Grinbaum A. Flow-cytometric light scattering measurement of red blood cell volume and hemoglobin concentration. Appl Opt 1985;24:1355–1365.
22. Semyanov KA, Tarasov PA, Soini JT, Petrov AK, Maltsev VP. Calibration free method to determine the size and hemoglobin concentration of individual red blood cells from light scattering. Appl Opt 2000;39:5884–5889.
23. Kolesnikova IV, Potapov SV, Yurkin MA, Hoekstra AG, Maltsev VP, Semyanov KA. Determination of volume, shape and refractive index of individual blood platelets. J Quant Spectrosc Radiat Transf 2006;102:37–45.
24. Strokotov DI, Yurkin MA, Gilev KV, van Bockstaele DR, Hoekstra AG, Rubtsov NB, Maltsev VP. Is there a difference between T- and B-lymphocyte morphology? J Biomed Opt 2009;14:064036.
25. Maltsev VP. Scanning flow cytometry for individual particle analysis. Rev Sci Instrum 2000;71:243–255.
26. Soini JT, Chernyshev AV, Hänninen PE, Soini E, Maltsev VP. A new design of the flow cuvette and optical set-up for the scanning flow cytometer. Cytometry 1998;31:78–84.
27. Surovtsev IV, Yurkin MA, Shvalov AN, Nekrasov VM, Sivolobova GF, Grazhdantseva AA, Maltsev VP, Chernyshev AV. Kinetics of initial stage of immunoagglutination studied with the scanning flow cytometer. Colloids Surf B 2003;32:245–255.
28. Chernyshev AV, Prots VI, Doroshkin AA, Maltsev VP. Measurement of scattering properties of individual particles with a scanning flow cytometer. Appl Opt 1995;34:6301–6305.
29. Gilev KV, Maltsev VP. Cytometry and Biokinetics Lab. Available at: http://cyto.kinetics.nsc.ru/. Accessed: April 25, 2011.
30. Maltsev VP, Semyanov KA. Characterisation of Bio-Particles from Light Scattering. Inverse and Ill-Posed Problems Series. Utrecht: VSP; 2004.
31. Hulst van de HC. Light Scattering by Small Particles. New York: Dover Publications, Inc; 1981. 470 p.
32. Collett E. Polarized Light: Fundamentals and Applications. New York: Marcel Dekker; 1993.
33. Yurkin MA, Semyanov KA, Tarasov PA, Chernyshev AV, Hoekstra AG, Maltsev VP. Experimental and theoretical study of light scattering by individual mature red blood cells by use of scanning flow cytometry and a discrete dipole approximation. Appl Opt 2005;44:5249–5256.
34. Jones DR, Pertunnen CD, Stuckman BE. Lipschitzian optimization without the Lipschitz constant. J Optim Theor Applicat 1993;79:157–181.
35. Ludlow IK, Everitt J. Application of Gegenbauer analysis to light-scattering from spheres: Theory. Phys Rev 1995;E51:2516–2526.
36. Ulanowski Z, Wang ZN, Kaye PH, Ludlow IK. Application of neural networks to the inverse light scattering problem for spheres. Appl Opt 1998;37:4027–4033.
37. Berdnik VV, Gilev K, Shvalov AN, Maltsev VP, Loiko VA. Characterization of spherical particles using high-order neural networks and scanning flow cytometry. J Quant Spectrosc Radiat Transf 2006;102:62–72.
38. Mishchenko MI, Travis LD, Mackowski DW. NASA GISS: Scattering—T-Matrix Codes. Available at: http://www.giss.nasa.gov/staff/mmishchenko/t_matrix.html. Accessed: April 25, 2011.
39. Chernyshev AV, Tarasov PA, Semianov KA, Nekrasov VM, Hoekstra AG, Maltsev VP. Erythrocyte lysis in isotonic solution of ammonium chloride: Theoretical modeling and experimental verification. J Theor Biol 2008;251:93–107.
40. Orlova DY, Yurkin MA, Hoekstra AG, Maltsev VP. Light scattering by neutrophils: Model, simulation, and experiment. J Biomed Opt 2008;13:054057.